Structural Engineering and Mechanics, *Vol. 48, No. 3 (2013) 395-414*
DOI: http://dx.doi.org/10.12989/sem.2013.48.3.395

Mechanical performance and design optimization of rib-stiffened super-wide bridge deck with twin box girders in concrete

Wen Xiong*[1], Jianshu Ye[1], Xuemei Gai[1] and C.S. Cai[2]

[1]*Department of Bridge Engineering, School of Transportation, Southeast University, Nanjing, 210096, China*
[2]*Department of Civil and Environmental Engineering, Louisiana State University, Baton Rouge, LA 70803, USA*

(Received May 17, 2013, Revised October 24, 2013, Accepted October 26, 2013)

Abstract. The present study fundamentally investigated the mechanical performance of the rib-stiffened super-wide bridge deck with twin box girders in concrete, which is a very popular application to efficiently widen the bridges with normal span. The shear lag effects of the specific cross-sections were firstly studied. The spatial stress distribution and local stiffness of the bridge deck with twin box girders were then investigated under several typical wheel load conditions. Meanwhile, a comparative study for the bridge deck with and without stiffening ribs was also carried out during the investigation; thereby, a design optimization for the stiffening ribs was further suggested. Finally, aiming at the preliminary design, an approximate methodology to manually calculate the bending moments of the rib-stiffened bridge deck was analytically proposed for engineers to quickly assess its performance. This rib-stiffened bridge deck with twin box girders can be widely applied for concrete (especially concrete cable-stayed) bridges with normal span, however, requiring a super-wide bridge width due to the traffic flow.

Keywords: twin box girders; super-wide bridge deck; stiffening ribs; concrete; mechanical performance; optimization

1. Introduction

Recently, concrete bridges with a super-wide bridge deck were widely designed and constructed to keep up with the continuous increase of the daily traffic. To build the bridge deck wider, the girder with separated twin boxes is currently becoming a very popular design option, which not only widens the bridge deck by splitting the girder box into two side-boxes but also significantly saves the cost of construction materials and gives many aero-dynamic advantages (Kim and Shim 2009, Ogawa *et al*. 2002, Larsena *et al*. 2007, Xiong *et al*. 2012). Such design especially fits when applied in cable-stayed bridges (i.e., Pasco-Kennewick bridge, U.S.A.), where the twin box can provide appropriate and economic anchorage spaces and areas for stay cables (Simões and Negrão 2000). However, this super-wide bridge deck design with the twin box girders usually represents high ratios of both width-to-span and width-to-height for bridge girders, which could potentially result in a super complicated stress distribution at cross-sections as well as a relatively weak local stiffness of bridge deck (Razaqpur and Li 1991, Ito 1996, Luo *et al*. 2004,

*Corresponding author, Assistant Professor, E-mail: wxiong12@gmail.com

http://www.techno-press.org/?journal=sem&subpage=8 ISSN: 1225-4568 (Print), 1598-6217 (Online)

Klowak and Mufti 2009, Xiong *et al*. 2012).

To address these problems, installing longitudinal stiffening ribs under bridge deck between twin boxes is one of the most popular solutions to keep or even improve the mechanical performance during the widening of bridge deck. The main idea behind is to design/build the bridge deck as an orthotropic plate, when loaded by vehicles, with a four-side boundary condition created by stiffening ribs and crossbeams. By doing this, the stiffness, strength, and stress distribution could be improved only with slight material increase. However, in the past decades most existing studies only focus on the steel rather than concrete bridge deck as a rib-stiffened orthotropic plate, and the steel deck is mainly applied in the super-long-span bridges (Overduin *et al*. 1999, Vincent and Ferro 2004, Pfeil *et al*. 2005, Medani 2006, Freitas *et al*. 2010). As a matter of fact, for the bridges with normal spans but super-wide width due to the busy traffic flow, the concrete materials are still the superior selection for constructing such stiffened wide bridge deck/girder and actually have already been applied in the practical engineering (Gimsing 1997, AASHTO 2004). Therefore, a detailed investigation is still desirable for such concrete stiffened bridge decks especially with twin box girders, which should also help create relative design theories or codes serving many bridges with super-wide width and normal span. It is noted that in the following study the components or structures discussed are all referring to that using concrete materials except special note.

In the present study, the mechanical performance of the rib-stiffened super-wide bridge deck with twin box concrete girders was fundamentally investigated using Finite Element Method (FEM). More specifically, the shear lag effects of the specific cross-sections were firstly studied. The spatial (three dimension) stress distribution and local stiffness of bridge deck with twin box girders were then investigated under several typical wheel load conditions. Meanwhile, a comparative study for the bridge deck with and without stiffening ribs was also carried out during the investigation; thereby, a design optimization for the stiffening ribs was further suggested. Finally, aiming at the preliminary design, an approximate methodology to determine the bending moments of rib-stiffened bridge decks was analytically proposed. It can be concluded that the rib-stiffened bridge deck with twin box girders should be a very good choice for the concrete (especially concrete cable-stayed) bridges with a normal span, however, requiring a super-wide bridge width due to the traffic flow.

2. Shear lag effects of bridge deck with twin box girders

To design the bridge wider, the twin boxes are connected separately by bridge deck as one single girder to undertake all the external loads including prestressing and cable forces. Following such a design, a significant shear lag effect could be easily predicted along the cross-sections and possibly generates structural cracks during both the construction and in-service periods (Gimsing 1997, Luo *et al*. 2004). This is not only a potential structural safety issue but also could negatively reduce the structural durability.

In the present study, a numerical investigation was conducted to illustrate the shear lag effects of the concerned bridge deck with twin box girders. All the investigations are given based on a significant dead-load condition of cable-stayed bridges, which is during the period with a maximum cantilever girder length before constructing the closure segment (Gimsing 1997). To distinguish the effects of the stiffening ribs, a comparative study was also carried out.

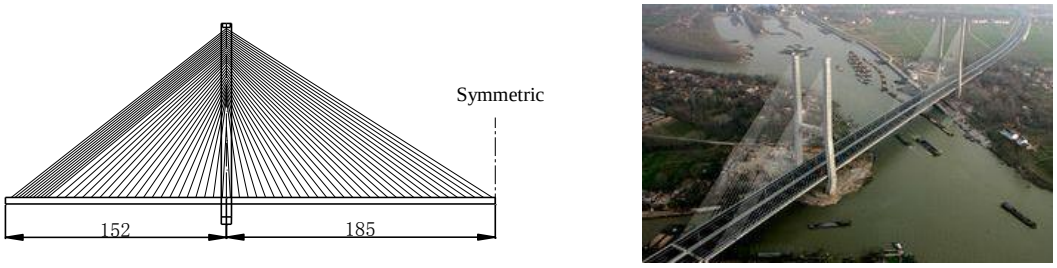

Fig. 1 Engineering drawing of design scheme and field photo of Wuhekou cable-stayed bridge (Unit: m)

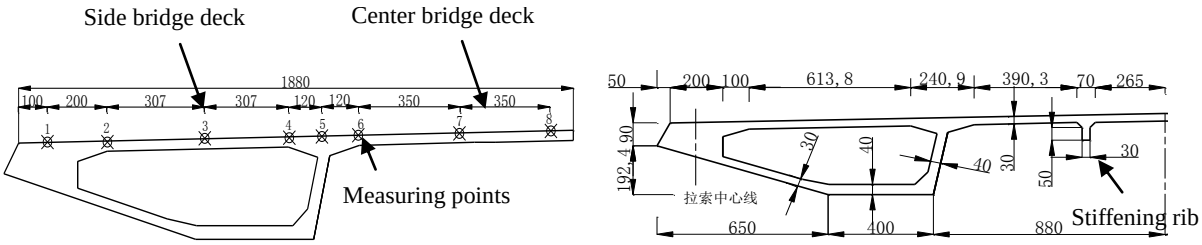

(a) Cross-section without stiffening ribs (b) Cross-section with stiffening ribs

Fig. 2 Selected cross-sections as investigation objects (herein only half cross-section is shown, unit: cm)

An existing cable-stayed bridge in China was taken as a typical example to demonstrate the shear lag effects of such bridge deck with twin box girders. The Wuhekou bridge (span arrangement: 152+370+152m), located at Jiangsu, China has the highest width-span ratio of 0.1043 in China (see Fig. 1). The cross-sections of the Wuhekou bridge are selected as the investigating objects in the following study as shown in Fig. 2(a) and 2(b) for the cases without and with stiffening ribs, respectively. Their geometrical measurements are also marked in Fig. 2.

Based on the engineering drawings, a Finite Element (FE) model with cross-sections shown in Fig. 2 was built by commercial program ANSYS using solid elements for girders (Elastic modulus, E=3.65×10^{4}MPa; Volume weight, γ=26kN/m^3), bridge deck (E=3.65×10^{4}MPa; γ=26kN/m^3), and pylon (E=3.5×10^{4}MPa; γ=26kN/m^3), which have three translational degrees-of-freedom (DOFs) for each node, and link elements for stay cables (E=1.95×10^{5}MPa; γ=83kN/m^3), which have two translational DOFs for each node, see Fig. 3. Applying a 3D solid FE model for the bridge makes it feasible to arrange measurement stations at the exact needed positions. Since the symmetry in the longitudinal direction, only half of the bridge was used in the present study to reduce the computation effort. The designed cable force is applied to each stay cable using iteration solutions provided by the ANSYS program, which ensures the bridge a good/safe condition during the construction period (Xiong *et al*. 2011).

Fig. 4 shows the stress distributions along the top layer of every selected cross-sections at the 1/4, 1/2, and 3/4 spans (labeled in Fig. 3), which are measured from eight points marked in Fig. 2(a). For a clear comparison, both the results with and without stiffening ribs are drawn in the same figures, where the plus represents tensile stress and minus means compressive stress. It should be noted that the stress results are shown for only half bridge deck in the transverse direction due to the symmetric design.

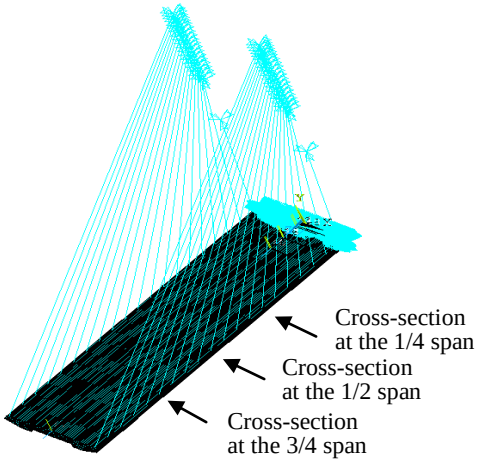

Fig. 3 Half FE model for the construction period with a maximum cantilever girder length

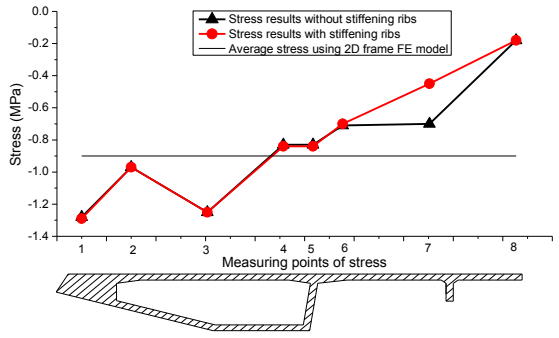

(a) Stress results at the 1/4 span

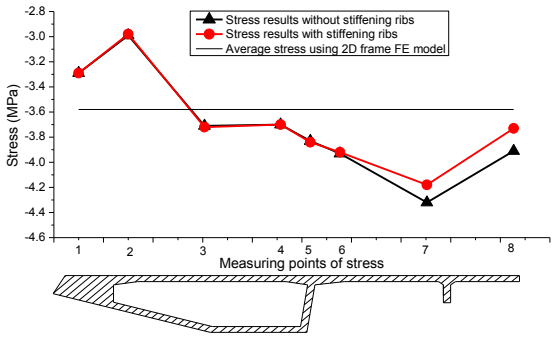

(b) Stress results at the 1/2 span

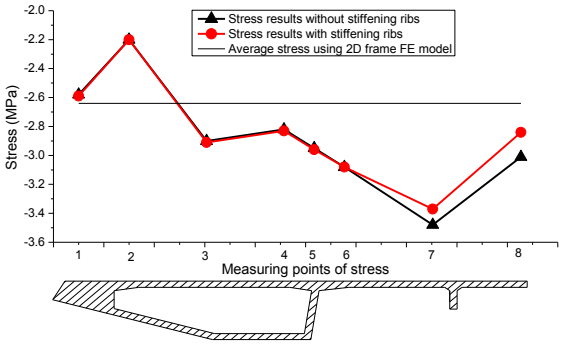

(c) Stress results at the 3/4 span

Fig. 4 Shear lag effects of cross-sections with/without stiffening ribs

From Fig. 4, it can be clearly observed that by the twin box design the stress distribution in the transverse direction, i.e., shear lag effects, on the top layer of bridge deck is significantly complicated especially subject to the possible cable force-induced torsion and bending. At the 1/2 and 3/4 spans, the longitudinal stresses at the center bridge deck (including measuring points 6~8,

Table 1 Comparative study on shear lag coefficients

Measuring points	Shear lag coefficient ***without*** stiffening ribs			Shear lag coefficient ***with*** stiffening ribs		
	L/4	L/2	3L/4	L/4	L/2	3L/4
1	1.42	0.92	0.98	1.42	0.92	0.98
2	1.08	0.84	0.83	1.07	0.83	0.83
3	1.39	1.04	1.10	1.37	1.04	1.10
4	0.92	1.03	1.07	0.92	1.03	1.07
5	0.92	1.07	1.12	0.92	1.07	1.12
6	0.79	1.10	1.17	0.77	1.09	1.17
7	0.78	1.21	1.32	0.49	1.17	1.28
8	0.20	1.09	1.14	0.20	1.04	1.08

Note: Herein the values of shear lag coefficient = Stress (computed by a 3D solid model) / average stress (computed by a 2D frame model)

see Fig. 2(a)) present much higher than those at the side bridge deck (including measuring points 1~5, see Fig. 2(a)). However, at the 1/4 span, the higher stresses oppositely move toward the center bridge deck while resulting in a different stress developing trend from other two cross-sections. This is mainly because the cross-section at the 1/4 span is located near to the pylon temporarily fixed with girder at construction stage, which could generate a unique boundary condition for the structure around that area. Actually, the boundary condition of cross-sections has been widely believed as the key factor to determine their shear lag effects.

Fig. 4 also implies a valuable reduction of longitudinal stresses by installing the stiffening ribs. Especially at the cross-section of 1/4 span, a 36% stress reduction can be found at measuring point 7. However, only the areas around the stiffening ribs present good results of stress reduction or re-distribution. In other words, the stiffening ribs do demonstrate an ability to weaken the shear lag effects however only limited in the nearby area of the ribs. The same conclusion can also be drawn by comparing their shear lag coefficients listed in Table 1. It should be noted the current rib arrangement may not cover all the possible designs. However, it can still provide a very reliable guidance for applying stiffening ribs in such a bridge deck. An optimized shear lag effect or stress distribution on the cross-sections can further be expected by a specific design using stiffening ribs (details can be found in Section 4).

3. Local behaviors of bridge deck under wheel loads

As an analytical model for design purpose, the bridge deck is usually regarded as a one-way slab, i.e., a plate/shell component with a boundary condition of two-side supports, see Fig. 5(a) (AASHTO 2004; JTG D62-2004 2004). When adding the stiffening ribs under bridge decks, this boundary condition could be thereby varied into a two-way slab with four-side supports, see Fig. 5(b). Using these two mechanical models, the local behaviors of bridge decks with twin boxes was fully investigated under an individual wheel load of vehicles. To be more accurate this wheel load is simulated as an area uniform load (contact area between the wheel and bridge deck surface) assigned by specific design codes. A comparative study on the cases with and without stiffening ribs was also given here.

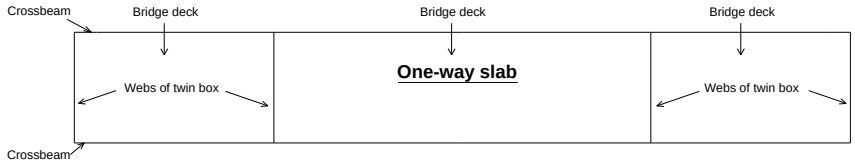

(a) Bridge deck without stiffening ribs

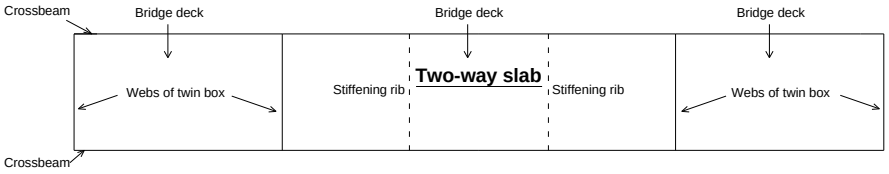

(b) Bridge deck with stiffening ribs

Fig. 5 Boundary condition of bridge deck

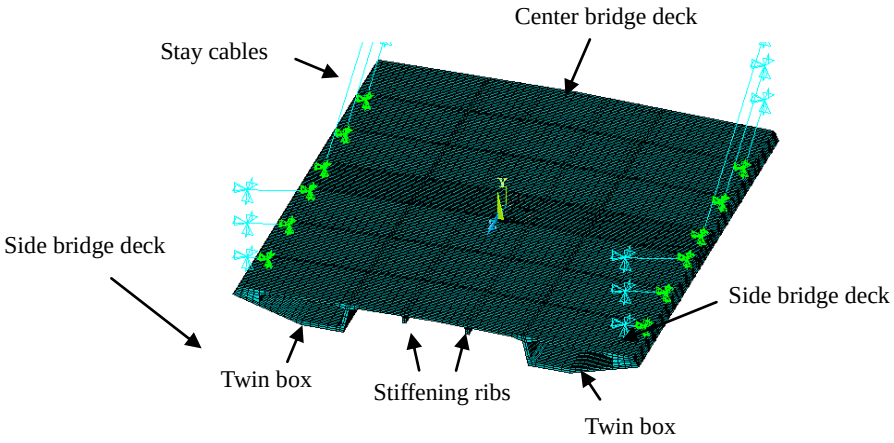

Fig. 6 FE model of seven girder segments

In the corresponding numerical analysis, a 3D solid FE model constituted of seven girder segments was built using the commercial program ANSYS based on Wuhekou bridge (the element and material properties keep the same as the previous study), see Fig. 6. Its boundary condition in terms of enforced deformations was applied based on the results of a 2D frame FE model. A single wheel load was assigned according to the Chinese specific bridge codes (JTG D62-2004 2004; JTG D60-2004 2004), which has 280kN of weight and 0.6m × 0.2m of contact area on bridge deck surface. Four typical load conditions regarding to different loading positions were finally considered in the present study which are numbered as cases 1~4 using a symbolized wheel load by a black solid rectangular in Fig. 7. The checked cross-sections in each load condition, are also pointed in Fig. 7 where the cross-sections 1-1~4-4 are selected to see the distribution of the longitudinal (normal) strain/stress along the longitudinal direction and the cross-sections A-A~B-B for the distribution of the transverse (normal) strain/stress along the transverse direction.

3.1 Results of case 1

The behavior of center bridge deck which is identified in both Figs. 6 and 7 was firstly

investigated using case 1 of wheel load. The contour results of normal strain and their exact values and corresponding measuring positions are given in Figs. 8 and 9, respectively. As a matter of convenience, Fig. 9 gives the data only from the top layer of bridge deck, where the plus represents tensile strain and minus means compressive strain.

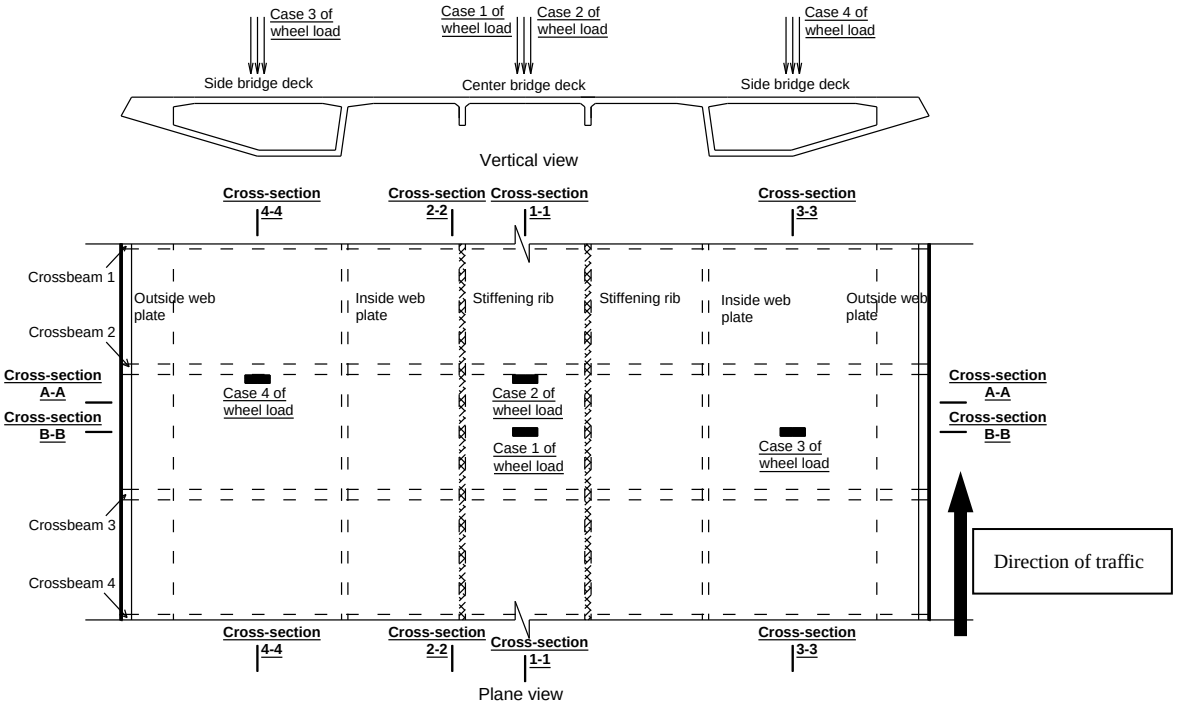

Fig. 7 Load cases and checked cross-sections

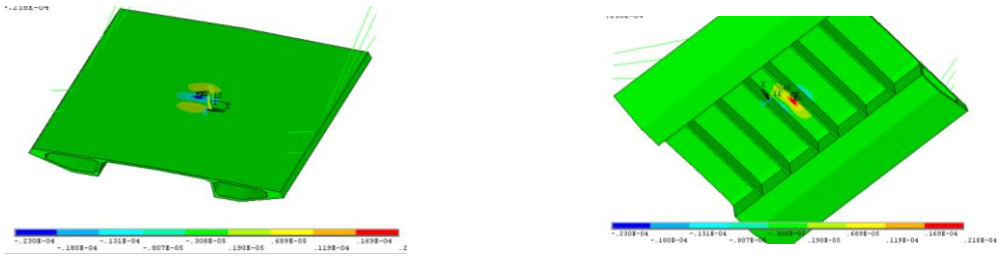

(a) Strain contours for bridge deck without stiffening ribs

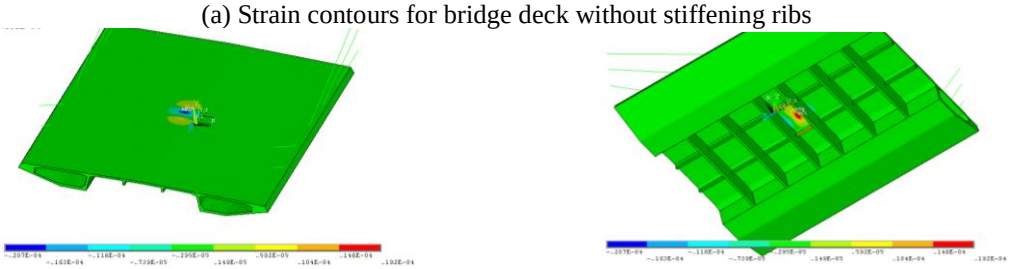

(b) Strain contours for bridge deck with stiffening ribs

Fig. 8 Normal strain contours under case 1

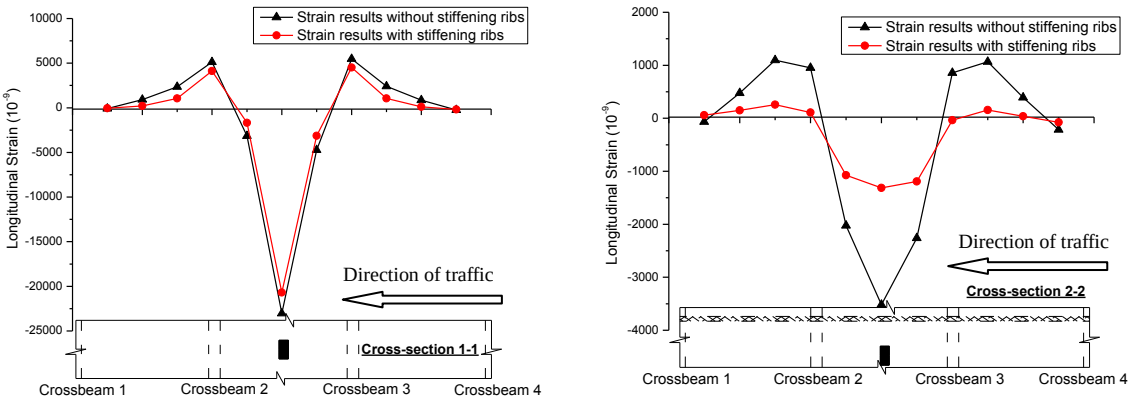

(a) Cross-section 1-1 (b) Cross-section 2-2

Fig. 9 Longitudinal strain in the top layer of bridge deck under case 1

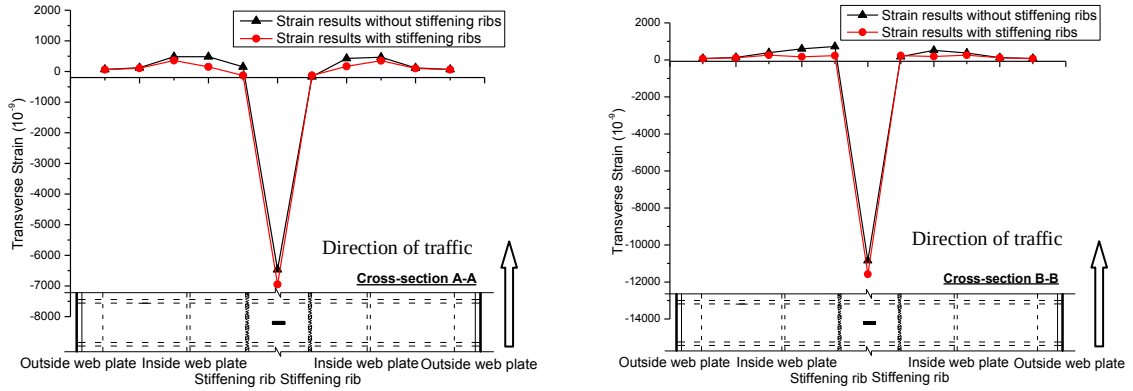

(a) Cross-section A-A (b) Cross-section B-B

Fig. 10 Transverse strain in the top layer of bridge deck in case 1

Similar longitudinal (normal) strain developing trends along the longitudinal direction can be clearly observed from the cross-section 1-1 and 2-2 shown in Fig. 9 by comparing the results with and without stiffening ribs. The peak of the longitudinal strain keeps the same position with the applying load in all cases and falls down significantly along both sides away from the load. As it can also be found that in such load case all the tensile strains appear in a limited area very close to the next-to-load crossbeams since the crossbeams as restricting supports can generate negative bending moments for the bridge deck there. In the same figures the phenomenon of strain reduction as well as its distribution smoothing can further be noticed after installing the stiffening ribs. Especially in cross-section 2-2 near the ribs, a 63% reduction can be generated for compression after stiffening and 96% for tensile case. However, unlike cross-section 2-2, the same remarkable reduction cannot be retained in cross-section 1-1 that is located far away from the stiffening ribs. This can be explained by that the stiffening effects from the ribs only have a limited influence area.

Fig. 10 shows the results of the transverse (normal) strain in cross-sections A-A and B-B which are both along the transverse direction of the bridge. Differed from longitudinal cases, few changes

by stiffening ribs can be found in this case no matter in strain value or developing trend. This is mainly because as a one-way slab (Fig. 5) installing stiffening ribs along the shorter span (longitudinal direction), which is the direction having strong bending stiffness, cannot significantly stiffen the bridge deck along a different direction (the transverse direction). Moreover in this case the installation happens to keep both stiffening ribs from the entire width of strain peak (see Fig. 10), which is further expected to make the stiffening effects worse. Actually it should be believed that a better mechanical improvement could be possibly achieved by re-arrange the stiffening ribs. In addition, around 50% reduction after stiffening can be observed for the tensile strain in the top layer of bridge deck, which is significantly helpful for the pavement design.

3.2 Results of case 2

In case 2 of wheel load, the longitudinal (normal) strain distribution along the longitudinal direction (cross-sections 1-1 and 2-2) and the transverse (normal) strain distribution along the transverse direction (cross-section A-A) are plotted in Figs. 11 and 12, respectively. The data in both figures are still measured from the top layer of bridge deck, where the plus represents tensile strain and minus means compressive strain.

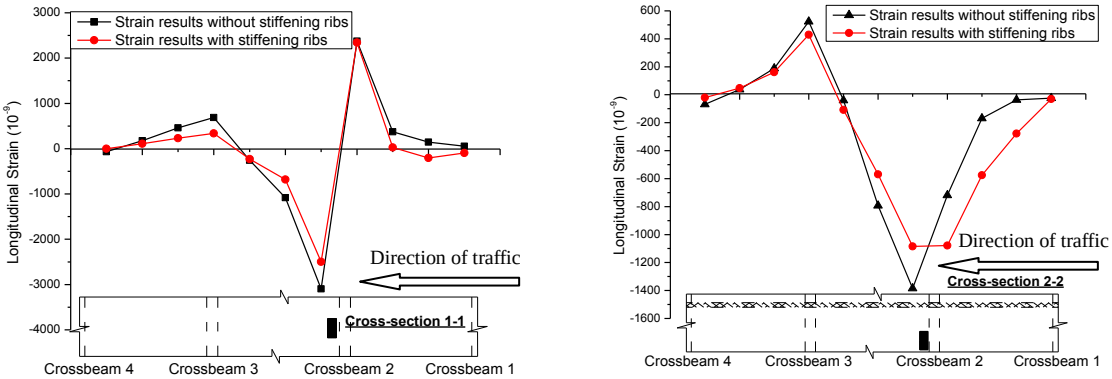

(a) Cross-section 1-1 (b) Cross-section 2-2

Fig. 11 Longitudinal strain in the top layer of bridge deck in case 2

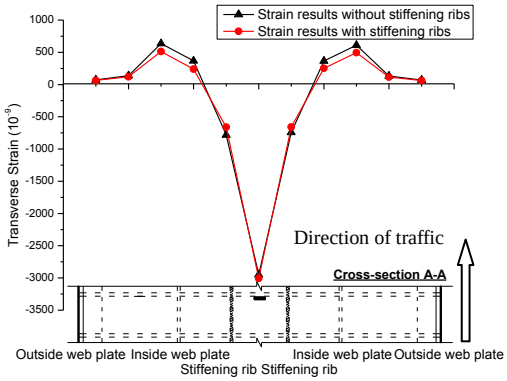

Cross-section A-A

Fig. 12 Transverse strain in the top layer of bridge deck in case 2

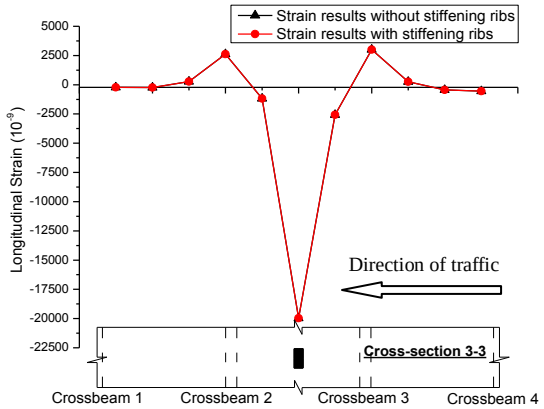

Cross-section 3-3

Fig. 13 Longitudinal strain in the top layer of bridge deck

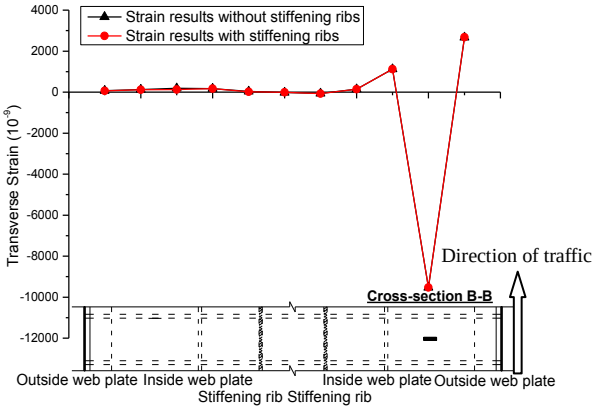

Cross-section B-B

Fig. 14 Transverse strain in the top layer of bridge deck

As expected, the wheel load applied next to one crossbeam in case 2 would force the strain peak toward the same crossbeam, as shown in Fig. 11. Except that both the longitudinal and transverse strains still follow similar distribution trends to that in previous case. In addition the change of applying position result in a remarkable reduction for all the strain values in the present case compared to those in case 1. Also in current case, the installation of stiffening ribs is still able to smooth the strain distribution in the longitudinal direction as good effects (Fig. 11) however not neccessary for the transverse strains due to the same reason discussed early (Fig. 12).

3.3 Results of case 3

Cases 3 and 4 of wheel load applied on the side bridge deck were also considered to investigate the mechanical performance of side bridge deck. After applying the wheel load as case 3 firstly, Figs. 13 and 14 plot the longitudinal (normal) strain distribution along the longitudinal direction (cross-sections 3-3) and the transverse (normal) strain distribution along the transverse direction (cross-section B-B).

From Figs. 13 and 14, it can be seen that in this case all the major mechanical responses are limited inside the side bridge deck. In the rest areas, almost nothing performance can be found (the strain values in those areas nearly equal to zero). It can also be observed that the stiffening ribs contribute little mechanical improvements for both center and side bridge deck since the stiffening ribs locate far away from the loading position. More visually speaking, the inside web plates would significantly “cut off” the stiffening path from center bridge deck, where the stiffening ribs locate, to side bridge deck, where the wheel load applies in this case.

3.4 Results of case 4

The results of case 4 are also given in Figs. 15 and 16, which as expected draws the same conclusion as case 3. No further explanation is given here for the page limits.

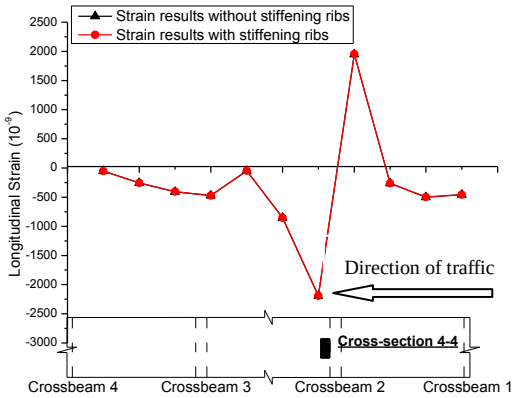

Cross-section 4-4

Fig. 15 Longitudinal strain in the top layer of bridge deck

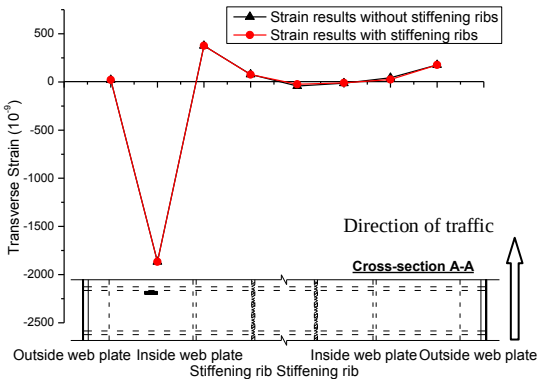

Cross-section A-A

Fig. 16 Transverse strain in the top layer of bridge deck

3.5 Summary of installing stiffening ribs

Based on the comparison above, the installation of stiffening ribs, in general, can lower the longitudinal strain and improve/smooth the strain distribution along the bridge deck. Unlike the longitudinal strain, however, only a few stiffening effects can be found for the transverse strain, only except the tensile one on the top layer of bridge beck which presents a good reduction in favor of pavement design (cases 1 and 2). It should be noted that the stiffening ribs only enhance the areas of bridge deck where they are installed and also directly under the load. For example, the side bridge deck cannot be stiffened by the stiffening ribs installed under the center bridge deck (cases 1 and 2) and the stiffened center bridge deck cannot, either, show a good improvement when the load moves to side bridge deck (cases 3 and 4).

In general, the installation of stiffening ribs creates bridge deck as a two-way slab from usual design as one-way slab, which can significantly optimize the boundary condition of bridge deck. Actually this better boundary with four-side restriction can also be seen as the essential origin for most mechanical improvements by stiffening ribs in the present study.

4. Optimal design of stiffening ribs

4.1 Comparative models of stiffening ribs

All the studies above were conducted based on a fixed design of stiffening ribs, which may not be the best choice. As matter of fact, the stiffening effects should possibly be adjusted by changing the geometrics of stiffening ribs. In order to address an optimal criterion, a series of parametric studies were theoretically carried out, which can also help further understand the stiffening behaviors from the ribs.

In practice the width of stiffening ribs is usually determined by the construction requirements including the diameter of steel reinforcement (12~32mm), space interval between two steel reinforcements (more than 30mm, two or three steel reinforcements applied), and depth of

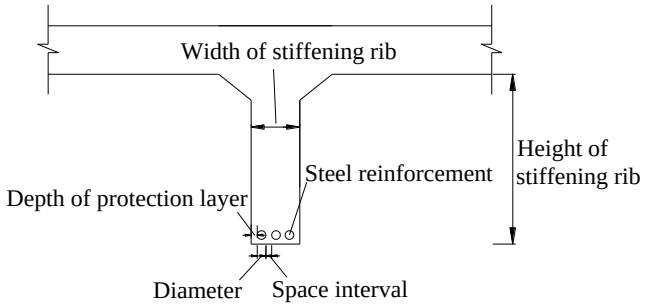

Fig. 17 Determination of the width of stiffening ribs

Table 2 Bending stiffness and stiffness ratio

Number	Dimension of stiffening ribs (width × height, mm)	Bending stiffness per unit width of bridge deck (Nm^2/m)	Bending stiffness per unit width of stiffening ribs (Nm^2/m)	Stiffness ratio R
1	300×300	8.213×10^7	8.213×10^7	1.00
2	300×400	8.213×107	1.947×10^8	2.37
3	300×500	8.213×107	3.802×10^8	4.63
4	300×600	8.213×107	6.570×10^8	8.00
5	300×700	8.213×107	1.043×10^9	12.70
6	300×800	8.213×107	1.557×10^9	18.96
7	300×900	8.213×107	2.217×10^9	26.99
8	300×1000	8.213×107	3.042×10^9	37.04

protection layer (more than 30mm), see Fig. 17. By adding them together, 300mm can be used as an unchanged width value in the following parametric study for stiffening ribs. Another geometric parameter, the height of stiffening ribs, therefore becomes variable (Fig. 17).

To cover more possible configurations of stiffening ribs, eight configurations with the same width of 300mm and different heights, 300mm, 400mm, 500mm, 600mm, 700mm, 800mm, 900mm, and 1000mm, respectively, were considered. The variable heights of stiffening ribs naturally make ribs have variable bending stiffness. In the present study, the ratio of bending stiffness of stiffening ribs to that of bridge deck (stiffness ratio for short hereafter) is applied as the final variable parameter in the following study. The bending stiffness per unit width of stiffening ribs and bridge deck can be calculated using $D_{rib} = Et^3/12$ (E = elastic modulus and t = height of stiffening ribs) and $D_{deck} = Eh^3/12$ (h = height of bridge deck), respectively. The variable parameter of stiffness ratio is then given by $R = D_{rib}/D_{deck}$, see Table 2. The basic FE model still keeps the same as the previous study. As a matter of convenience, a single wheel load is applied on the center of center bridge deck following case 1 of wheel load in Fig. 7. This load condition evidently shows how the stiffening ribs perform.

4.2 Results of analysis

Using these eight configurations, several mechanical parameters were investigated by varying the variable heights from 300mm to 1000mm, i.e., stiffness ratio from 1 to 37.04 (see Table 2). Corresponding results are given in Figs. 18~20.

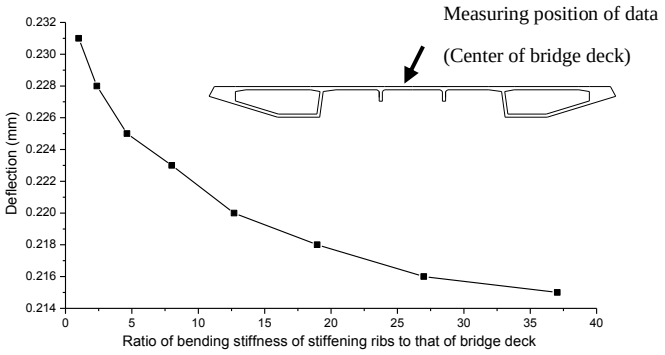

Fig. 18 Deflection vs stiffness ratios

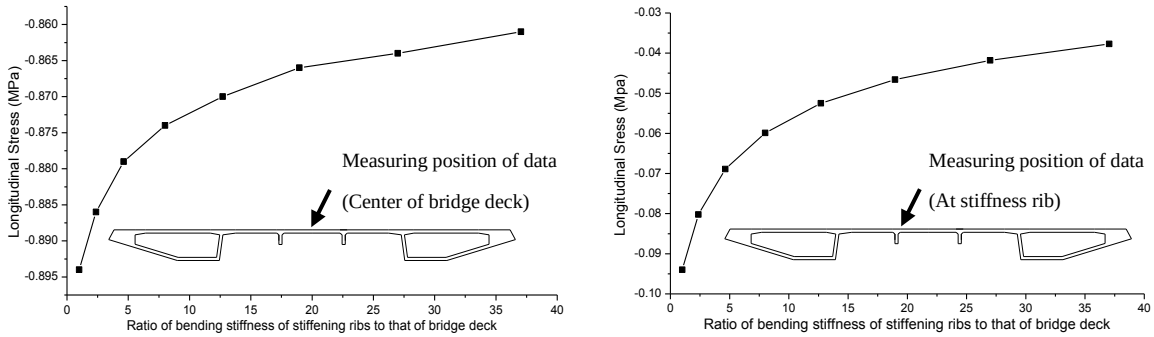

(1) Stress at the center of bridge deck (2) Stress of bridge deck at stiffening rib

Fig. 19 Longitudinal stress (minus denotes compression) vs stiffness ratios

Fig. 18 shows the deflection at the center of bridge deck along with the varying stiffness ratio from 1 to 37.04. A continuous downward trend of deflection, i.e., an increasing bending stiffness of the stiffened bridge deck, can be clearly observed as the stiffness ratio increases. However, when the stiffness ratio becomes greater than around 13, the deflection curve becomes flatter and flatter. In other words, values over 13 of stiffness ratio do not necessarily provide a remarkable stiffness improvement. Therefore, 13 can be regarded as a good value for stiffness ratio with both enhanced stiffness and good economical behavior.

From the stress results shown in Fig. 19, no matter at the center of bridge deck or stiffening rib, similar developing trends can be found after comparing both curves, where the absolute longitudinal stresses continuously drop down along with an increasing stiffness ratio. A key point of around 10 of stiffness ratio can also be given and thereafter the mechanical improvement by increasing stiffness ratio becomes low-efficient. This value of 10 can be further considered as another optimal value of stiffness ratio from the viewpoint of longitudinal stress.

When it comes to the transverse stress, an increasing stiffening ratio is still able to lower the compressive stress at the center of bridge deck (Fig. 20(a)); however, at stiffening ribs it presents unlikely tensile stresses with an increasing trend after increasing the stiffening ratio (Fig. 20(b)). Moreover, the stress variation shown in Fig. 20(a) is much slighter than it is in Fig. 20(b). Therefore, a lower stiffness ratio is preferred since it is able to reduce the transverse stress of bridge deck at stiffening ribs only resulting in a slight transverse stress rising (the absolute values) at the center of bridge deck.

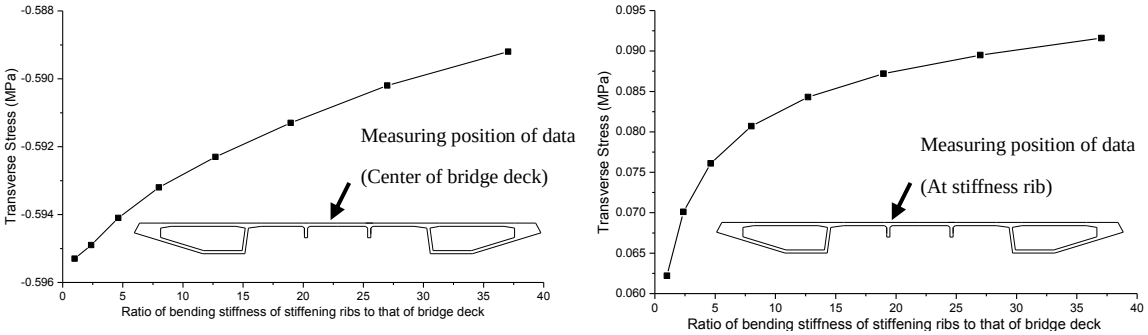

(a) Stress at the center of bridge deck (b) Stress of bridge deck at stiffening rib

Fig. 20 Transverse stress (minus denotes compression) vs stiffness ratios

Table 3 Appropriate values of stiffness ratio

Mechanical behaviors	Criterion	Appropriate values of stiffness ratio
Deflection	The higher is preferred	Around 13
Longitudinal stress	The lower is preferred	Around 10
Transverse stress	The lower is preferred	The lower, the better

It should be noted that all the results in Figs. 18~20 are given based on applying a single wheel load and only two stiffened ribs, which are possibly not in accordance with the real traffic conditions. However, all the developing trends of the concerned mechanical performances, rather than the data values, in the present study should be correct.

4.3 Summary of optimal design

As a matter of fact, using only one specific value for stiffness ratio cannot guarantee a satisfactory result for all the investigated mechanical parameters (deflection, longitudinal stress, and transverse stress). It becomes more complicated if both the constructional and economical performances need to be satisfied simultaneously, which may lead to a completely different way of selecting the appropriate stiffness ratio from the ways govern by the mechanical parameters. The appropriate values of stiffness ratio for all three mechanical parameters using the eight analytical models of stiffening ribs are summarized in Table 3.

From Table 3, it can be seen that it is truly difficult to select one specific value to achieve an optimal performance for the bridge deck regarding to all the mechanical parameters; however, an appropriate range can still be determined to achieve a good balance among the deflection (stiffness of bridge deck), longitudinal and transverse stresses. In the present study, by comparing the stiffness ratio values summarized in Table 3 a range of 8 to 12 (Dimension of stiffening ribs: 300x600~300×700mm) is considered as an appropriate range, taking all concerned performances into account.

It is noted that such optimal conclusion is drawn only based on a fixed arrangement for the stiffening ribs (only two ribs installed by a fixed interval span), as shown in Fig. 7. However, this conclusion of optimal design should also be acceptable for stiffening ribs with different interval spaces or different numbers of ribs. This is mainly because in most conditions the stiffening rib works individually in each own area and the stiffening effects are determined mostly by its own

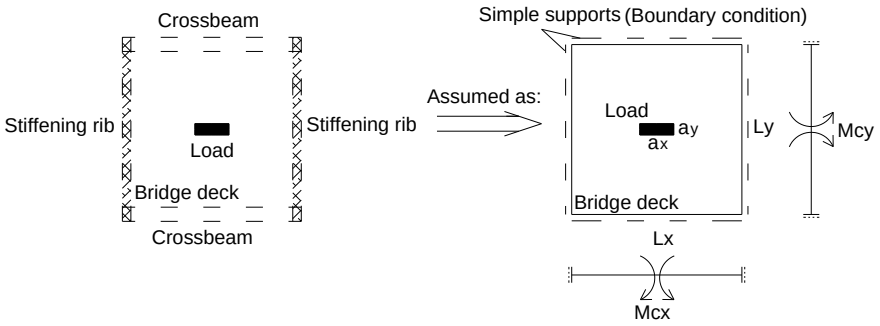

Fig. 21 Boundary condition of bridge deck

geometric dimension. After designing the ribs as the appropriate values of stiffness ratio, the optimization effect can further be enhanced through changing the interval spaces or different numbers of ribs.

5. Approximate calculation on bending moments

Although the stress/strain of the loaded bridge deck can be conveniently obtained using FE method, the internal forces such as bending moments of bridge deck are still hard to be directly known, which however are very desirable especially during the preliminary design. In the present study a simple solution for determining the bending moments of bridge deck is analytically proposed using a two-way slab model, which should be very suitable for manual calculation.

5.1 Bending moments of bridge deck at center span

As mentioned early, in every load cases the mechanical response of bridge deck drops significantly and very quickly even till almost zero when approaching to the stiffening ribs or crossbeams. As such, the boundary condition of the bridge deck as a two-way slab can be safely simplified into a four-side simple support, see Fig. 21.

As the model of Fig. 21, M_{cx} and M_{cy} can be conveniently expressed using Eqs. (1) and (2), which represent the bending moments at center span of bridge deck along the transverse and longitudinal directions, respectively, in each girder segment (see Fig. 21). A central wheel load shown in Fig. 21 is also applied, which causes one of the worst load conditions.

$$M_{cx}=k_{0x}\times q_c\times a_x\times a_y \quad \text{(unit: N·m/m)} \tag{1}$$

$$M_{cy}=k_{0y}\times q_c\times a_x\times a_y \quad \text{(unit: N·m/m)} \tag{2}$$

where M_{cx} and M_{cy} = bending moments at center span of bridge deck along the transverse and longitudinal directions, respectively, in each girder segment (Fig. 21); k_{0x} and k_{0y}= coefficients of M_{cx} and M_{cy}, respectively, the values of which can be determined from an existing coefficient table (Table 4) depending on different values of L_x, L_y, a_x, and a_y (Fig. 21); L_x and L_y = length and width of bridge deck, respectively; q_c = density of the area load (wheel load); and a_x and a_y = length and width of the area load, respectively.

Table 4 Coefficient table of k_{0x} and k_{0y} (v= 0)

L_y/L_x	a_x/L_x	k_{0x} (M_{cx})						k_{0y} (M_{cy})					
	a_y/L_y	0.0	0.2	0.4	0.6	0.8	1.0	0.0	0.2	0.4	0.6	0.8	1.0
1.0	0.0	-	0.1746	0.1213	0.0920	0.0728	0.0592	-	0.2528	0.1957	0.1602	0.1329	0.1097
	0.2	0.2528	0.1634	0.1176	0.0900	0.0714	0.0581	0.1746	0.1634	0.1434	0.1236	0.1049	0.0872
	0.4	0.1957	0.1434	0.1083	0.0843	0.0674	0.0549	0.1213	0.1176	0.1083	0.0962	0.0831	0.0693
	0.6	0.1602	0.1236	0.0962	0.0762	0.0613	0.0500	0.0920	0.0900	0.0843	0.0762	0.0664	0.0556
	0.8	0.1329	0.1049	0.0831	0.0664	0.0537	0.0439	0.0728	0.0714	0.0674	0.0613	0.0537	0.0451
	1.0	0.1097	0.0872	0.0693	0.0556	0.0451	0.0368	0.0592	0.0581	0.0549	0.0500	0.0439	0.0368
1.2	0.0	-	0.1936	0.1394	0.1086	0.0874	0.0714	-	0.2456	0.1889	0.1540	0.1274	0.1051
	0.2	0.2723	0.1826	0.1358	0.1066	0.0861	0.0704	0.1673	0.1563	0.1367	0.1174	0.0995	0.0826
	0.4	0.2156	0.1630	0.1268	0.1013	0.0824	0.0675	0.1143	0.1107	0.1017	0.0903	0.0778	0.0650
	0.6	0.1807	0.1438	0.1154	0.0936	0.0767	0.0629	0.0854	0.0835	0.0782	0.0706	0.0615	0.0515
	0.8	0.1543	0.1259	0.1029	0.0845	0.0696	0.0572	0.0670	0.0657	0.0620	0.0565	0.0495	0.0415
	1.0	0.1322	0.1093	0.0902	0.0745	0.0616	0.0507	0.0544	0.0534	0.0506	0.0463	0.0406	0.0341
	1.2	0.1126	0.0934	0.0773	0.0640	0.0530	0.0436	0.0455	0.0447	0.0424	0.0388	0.0341	0.0286
1.4	0.0	-	0.2063	0.1515	0.1197	0.0972	0.0796	-	0.2394	0.1829	0.1485	0.1226	0.1010
	0.2	0.2854	0.1954	0.1480	0.1178	0.0960	0.0787	0.1610	0.1500	0.1308	0.1120	0.0947	0.0786
	0.4	0.2289	0.1761	0.1393	0.1128	0.0925	0.0760	0.1080	0.1045	0.0958	0.0849	0.0731	0.0609
	0.6	0.1946	0.1574	0.1283	0.1055	0.0872	0.0718	0.0792	0.0774	0.0724	0.0653	0.0568	0.0476
	0.8	0.1690	0.1403	0.1166	0.0970	0.0806	0.0665	0.0608	0.0597	0.0563	0.0512	0.0449	0.0377
	1.0	0.1478	0.1246	0.1047	0.0878	0.0733	0.0606	0.0485	0.0476	0.0452	0.0413	0.0362	0.0305
	1.2	0.1294	0.1099	0.0929	0.0783	0.0655	0.0542	0.0400	0.0394	0.0374	0.0342	0.0301	0.0253
	1.4	0.1126	0.0959	0.0813	0.0685	0.0574	0.0475	0.0342	0.0336	0.0319	0.0292	0.0257	0.0216
1.6	0.0	-	0.2144	0.1592	0.1267	0.1034	0.0849	-	0.2348	0.1786	0.1445	0.1191	0.0981
	0.2	0.2937	0.2036	0.1558	0.1250	0.1023	0.0840	0.1563	0.1455	0.1264	0.1080	0.0912	0.0756
	0.4	0.2375	0.1845	0.1473	0.1201	0.0989	0.0814	0.1033	0.0998	0.0914	0.0808	0.0695	0.0579
	0.6	0.2035	0.1662	0.1367	0.1132	0.0939	0.0774	0.0744	0.0726	0.0679	0.0612	0.0532	0.0445
	0.8	0.1784	0.1497	0.1255	0.1052	0.0878	0.0725	0.0560	0.0549	0.518	0.0470	0.0412	0.0346
	1.0	0.1580	0.1346	0.1143	0.0966	0.0810	0.0670	0.0436	0.0428	0.0405	0.0370	0.0325	0.0273
	1.2	0.1405	0.1208	0.1033	0.0878	0.0739	0.0612	0.0351	0.0345	0.0327	0.0299	0.0264	0.0222
	1.4	0.1248	0.1079	0.0926	0.0790	0.0666	0.0552	0.0292	0.0288	0.0273	0.0250	0.0221	0.0185
	1.6	0.1105	0.0956	0.0822	0.0702	0.0592	0.0491	0.0253	0.0249	0.0237	0.0217	0.0191	0.0161

In this coefficient table, all the values of k_0 were calculated with the consideration of v (Poisson's ratio) = 0. If v has different values, M_{cx} and M_{cy} need to be adjusted as

$$M_{cx}^{v} = M_{cx} + vM_{cy} \quad \text{(unit: N·m/m)} \tag{3}$$

$$M_{cy}^{v} = M_{cy} + vM_{cx} \quad \text{(unit: N·m/m)} \tag{4}$$

5.2 Bending moments of bridge deck at crossbeams or stiffening ribs

Following the same analytical model above, the bending moments of bridge deck at crossbeams or stiffening ribs should be zero since they are at the boundary of simple support, which are

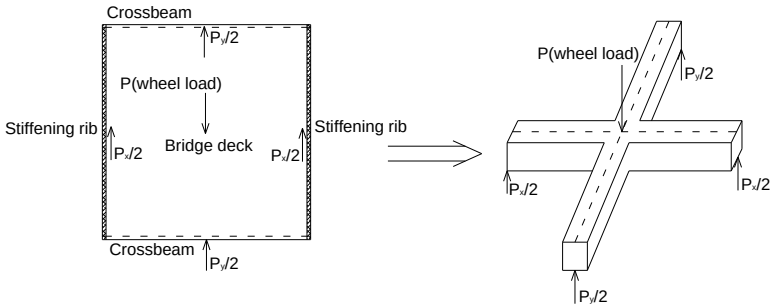

Fig. 22 Analytical model of bridge deck

obviously not consistent to the reality. Therefore, to obtain the bending moments here requires a different analytical model.

Actually, under central wheel load, the bridge deck as a two-way slab is more likely to split the wheel load into two parts and transit them along both the longitudinal and transverse directions, as shown in Fig. 22.

Based on this analytical model, the central deflections of the transverse and longitudinal "girders/beams" (see right side of Fig. 22) can be mathematically described as follows

$$\Delta_x = k_x(P_x L_x^3/EI) \tag{5}$$

$$\Delta_y = k_y(P_y L_y^3/EI) \tag{6}$$

where Δ_x and Δ_y = central deflections of the transverse and longitudinal "girders/beams", respectively; k_x and k_y= coefficients of Δ_x and Δ_y, respectively, the values of which are determined by boundary conditions; P_x and P_y = components of wheel load P split along the longitudinal and transverse directions, respectively; E = elastic modulus; and I = moment of inertia.

Since $\Delta_x = \Delta_y$ and $P = P_x + P_y$, P_x and P_y can be calculated as

$$P_x = \frac{k_y L_y^3}{k_x L_x^3 + k_y L_y^3} P \tag{7}$$

$$P_y = \frac{k_x L_x^3}{k_x L_x^3 + k_y L_y^3} P \tag{8}$$

From Eqs. (7) and (8), it can be seen that P_x and P_y are interrelated with the boundary conditions (k_x and k_y) and length/width of bridge deck (L_x and L_y). If let k_x equal to k_y (this assumption is also applied in the bridge design code of AASHTO), Eqs. (7) and (8) can be further written as

$$P_x = \frac{L_y^3}{L_x^3 + L_y^3} P \tag{9}$$

$$P_y = \frac{L_x^3}{L_x^3 + L_y^3} P \tag{10}$$

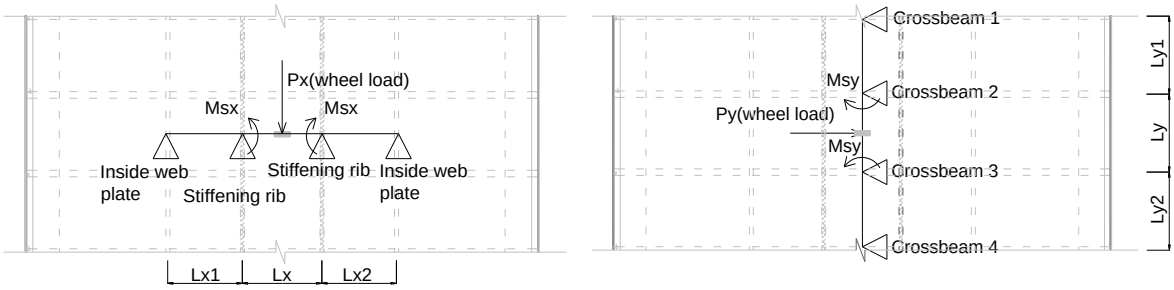

Fig. 23 Simplified model of bridge deck

Table 5 Accuracy verification

Types of bending moments	FE method (N·m/m)	Proposed method (N·m/m)	Difference
M_{cx}	7567	9084	20%
M_{cy}	12127	14268	15%
M_{sx}	-2092	-1800	-14%
M_{sy}	-3802	-2950	-22%

Then, simplifying the bridge deck into two continuous girders along the transverse and longitudinal directions where P_x and P_y are centrally applied, respectively, only three "spans" for each simplified girder are considered to assure good results and also make the calculation simple, see Fig. 23. By doing this, the bending moments of bridge deck at stiffening ribs or crossbeams, i.e., M_{sx} and M_{sy} in Fig. 23, respectively, can be approximately calculated based on simple continuous girder structures with three spans. If $L_x=L_{x1}=L_{x2}$ and $L_y=L_{y1}=L_{y2}$ (see Fig. 23), M_{sx} and M_{sy} can be further simplified as

$$M_{sx}=0.075P_xL_x/L_y \quad \text{(unit: N·m/m)} \tag{11}$$

$$M_{sy}=0.075P_yL_y/L_x \quad \text{(unit: N·m/m)} \tag{12}$$

5.3 Accuracy verification

The accuracy of bending moment calculation using the proposed methodology is simply verified by comparing them to the "accurate" values from FE method. The verification results are shown in Table 5 and from the results it is seen that the accuracy of the proposed methodology could be fully acceptable in the preliminary stage of bridge design. Especially for the key parameters of M_{cx} and M_{cy} usually controlling the design, slight overestimation by the proposed approximate methodology could well assure the design safe and conservative.

5.4 Summary of bending moment calculation

So far, the bending moments of bridge deck, no matter at center span, crossbeams or stiffening ribs, can be manually calculated under a central wheel load which is one of the most important load conditions. For other cases with different wheel load positions, the bending moments become significantly weak and can also be simply calculated using the same model of bridge deck in Fig. 23. If two or more wheel loads need to be considered, the superposition law can be directly applied

to add each result together from every wheel loads.

The accuracy of the proposed approximate methodology is clearly good enough in the preliminary stage of bridge design. Its advantages of manual calculation and time-saving can further assure this methodology practical and convenient for engineers to quickly assess the performance of the rib-stiffened super-wide bridge deck with twin box girders.

6. Conclusions

The present study fundamentally investigated the mechanical performances of the rib-stiffened super-wide bridge deck with twin box girders in concrete. Since the character of super-wide structure, the shear lag effects of the cross-sections were firstly studied. The spatial (three dimension) stress distribution and local stiffness of such bridge deck were also investigated. A comparative study for the bridge deck with and without stiffening ribs was meanwhile carried out and thus results in a design optimization for the stiffening ribs. Finally, aiming at the preliminary design, an approximate methodology to manually calculate the bending moments of rib-stiffened bridge deck was analytically proposed for engineers to quickly assess its performance. This rib-stiffened bridge deck with twin box girders can be widely applied for the concrete (especially concrete cable-stayed) bridges with normal span, however, requiring a super-wide bridge width due to the traffic flow.

It should be pointed out that the possible errors with FE simulation and limit cases during the investigation may affect the conclusions drawn in the present study. However, solutions to these problems are now available by an ongoing laboratory experiment of the bridge deck model installing strain/deflection measurement devices. In summary, the present study provides some practical conclusions for the mechanical performances of the rib-stiffened super-wide bridge deck with twin box girders, which should be very useful and convenient in the preliminary bridge design.

Acknowledgments

The financial supports for this work from the National Natural Science Foundation of China (Project No. 51208097 and 51229801), Specialized Research Fund for the Doctoral Program of Higher Education of China (Project No. 20120092120058), and Natural Science Foundation of Jiangsu Province of China (Project No. BK2012343) are gratefully acknowledged. The opinions and statements do not necessarily represent those of the sponsors.

References

Ogawa, K., Shimodoi, H. and Oryu, T. (2002), "Aerodynamic characteristics of a 2-boxgirder section adaptable for a super-long span suspension bridge", *Journal of Wind Engineering and Industrial Aerodynamics*, **90**(12-15), 2033-2043.

Kim, H.H. and Shim, C.S. (2009), "Experimental investigation of double composite twin-girder railway bridges", *Journal of Constructional Steel Research*, **65**(6), 1355-1365.

Larsena, A., Savageb, M., Lafrenièreb, A., Hui, M.C.H. and Larsen, S.V. (2007), "Investigation of vortex response of a twinbox bridge section at high and low Reynolds numbers", *Journal of Wind Engineering*

and Industrial Aerodynamics, **96**(6-7), 934-944.
Xiong, W., Xiao, R.C., Deng, L. and Cai, C.S. (2010), "Methodology of long-term real-time condition assessment for existing cable-stayed bridges", *Advances in Structural Engineering*, **13**(1), 111-125.
Razaqpur, A.G. and Li, H.G. (1991), "A finite element with exact shape functions for shear lag analysis in multi-cell box girders", *Computers and Structures*, **39**(1-2), 155-163.
Ito, M. (1996), "Cable-supported steel bridges: design problems and solutions", *Journal of Constructional Steel Research*, **39**(1), 69-84.
Simões, L.M.C. and Negrão, J.H.J.O. (2000), ''Optimization of cable-stayed bridges with box-girder decks", *Advances in Engineering Software*, **31**(6), 417-423.
Klowak, C.S. and Mufti, A.A. (2009), "Behaviour of bridge deck cantilever overhangs subjected to a static and fatigue concentrated load", *Construction and Building Materials*, **23**(4), 1653-1664.
Luo, Q.Z., Wu, Y.M., Li, Q.S., Tang, J., and Liu, G.D. (2004), "A finite segment model for shear lag analysis", *Engineering Structures*, **26**(14), 2113-2124.
Freitas, S.T.D., Kolstein, H. and Bijlaard, F. (2010), "Composite bonded systems for renovations of orthotropic steel bridge decks", *Composite Structures*, **92**(4), 853-862.
Medani, T.O. (2006), "Design principles of surfacings on orthotropic steel bridge decks", PhD Thesis, Delft University of Technology, Delft, The Netherlands.
Overduin, L., Romeijn, A. and Kolstein, M.H. (1999), "Modelling of bridge deck systems for orthotropic steel bridges", *Proceedings National Conference on ComputationalMmechanics*, Volos, Greece.
Vincent, R. and Ferro, A. (2004), "A new orthotropic bridge deck: design, fabrication and construction of the shenley bridge incorporating an SPS orthotropic bridge deck", *2004 International Orthotropic Bridge Conference*, Sacramento, California, USA.
Pfeil, M.S., Battista, R.C. and Mergulhão, A.J.R. (2005), "Stress concentration in steelbridge orthotropic decks", *Journal of Constructional Steel Research*, **61**(8), 1172-1184.
Gimsing, N.J. (1997), *Cable-Supported bridges*, 2nd edition, John Wiley & Sons, New York, U.S.A.
AASHTO LRFD Bridge Design Specifications (2004), Association of state highway and transportation officials, Washington, DC, U.S.A.
Xiong, W., Cai, C.S., Zhang, Y. and Xiao, R.C. (2011), "Study of super long span cable-stayed bridges with CFRP components", *Engineering Structures*, **33**(2), 330-343.
JTG D60-2004 (2004), "General Code for Design of Highway Bridges and Culverts", China Communications Press, Beijing, China.
JTG D62-2004 (2004), "Code for Design of Highway Reinforced Concrete and Prestressed Concrete Bridges and Culverts", China Communications Press, Beijing, China.